Classical and quantum chaos of the wedge billiard. II. Quantum mechanics and quantization rules

T. Szeredi and D. A. Goodings
Department of Physics and Astronomy, McMaster University, Hamilton, Ontario, Canada L8S 4M1
(Received 2 December 1992)

In this second of two papers on the classical-quantum correspondence of the wedge billiard, attention is focused on testing a number of quantization schemes based on the Gutzwiller periodic-orbit theory. To begin with, accurate values of the energy eigenvalues of the Schrödinger equation for the 49° wedge and the 60° wedge have been calculated by means of a large matrix diagonalization. These are used to judge the success of various approaches to the problem of determining approximate semiclassical energy eigenvalues, knowing only the characteristics of the periodic orbits of the classical system. First, it is shown that the periodic-orbit sum of the Gutzwiller trace formula is not absolutely convergent for either the 49° wedge or the 60° wedge. Nevertheless, the periodic-orbit sum may be conditionally convergent. For the 60° wedge, a calculation including 1621 primitive periodic orbits yields peaks that are close to the lowest 20 eigenvalues of the Schrödinger equation. Results for the 49° wedge are less successful, however. It is shown that the infinite families of primitive periodic orbits with nearly the same action, described in the preceding paper, cannot be treated in the usual way by the stationary-phase approximation. Finally, a number of quantization rules based on the staircase function and on the zeros of the dynamical ζ function are studied. The Riemann-Siegel look-alike equation is found to give good results for the lowest 20 energy eigenvalues of the 49° wedge, but misses several pairs of eigenvalues over the range of the next 30 eigenvalues. However, the smoothed version of this equation, formulated by Berry and Keating, gives good results for all the energy eigenvalues over the range of the lowest hundred eigenvalues. Even better results are found when the functional equation is combined with the dynamical ζ function expressed as a simple product over about a thousand primitive periodic orbits. Surprisingly, the best results of all are obtained from the zeros of Bogomolny's functional determinant making use of only 16 irreducible orbits.

PACS number(s): 05.45.+b, 03.20.+i, 03.65.−w

I. INTRODUCTION

This paper reports a study of the classical-quantum correspondence for a classically chaotic system called the wedge billiard. The system was described in the preceding paper (to be referred to as I) which was mainly concerned with the periodic orbits of the classical motion. It is known that if the wedge angle ϕ is greater than 45°, the classical system exhibits hard chaos, meaning that a positive Lyapunov exponent exists for every classical trajectory and all the periodic orbits of the system are unstable. Our main interest will be in exploring a variety of ways of obtaining accurate energy eigenvalues of the quantum system from a detailed knowledge of the primitive periodic orbits of the classical system.

The indispensable tool for carrying out this study is the Gutzwiller trace formula for the spectral density [1, 2], together with relations derived from it such as the spectral staircase function and the dynamical ζ function. In an earlier paper on the wedge billiard [3] we derived a damped sine or cosine Fourier transform of the Gutzwiller relation and showed that the quantum energy eigenvalues can be used to obtain quantitative information about the periodic orbits of the classical system. Here, however, we focus our attention on finding the best way to proceed in the opposite direction, from the classical periodic orbits to the quantum energy eigenvalues. Our work is similar to the detailed investigations of other nonintegrable Hamiltonian systems—the anisotropic Kepler problem [4–7], the Hadamard-Gutzwiller model for a particle moving on a surface of constant negative curvature [8–10], and the hyperbola billiard [11–14].

The plan of the paper is as follows. In order to judge the success of the various approaches described later in the paper, one needs to have accurate values for the energy eigenvalues of the quantum system. Our method of calculating these eigenvalues of the time-independent Schrödinger equation is described in the next section. In the following section we present the distributions of the energy spacings of the 49° and 60° wedges and compare them with the distribution for a Gaussian orthogonal ensemble. In Sec. IV we show that the Gutzwiller periodic-orbit sum is not absolutely convergent for either the 49° wedge or the 60° wedge. Nevertheless, when the sum is truncated at one or two thousand primitive periodic orbits, it is found to give peaks lying close to the first 11 eigenvalues of the 49° wedge and the first 20 eigenvalues of the 60° wedge. The effects due to infinite families of primitive periodic orbits with nearly the same action are discussed in Sec. V, where it is shown that such families cannot be treated by the stationary-phase approximation in the usual way. In Sec. VI we consider a quantization rule based on the staircase function obtained by integrating the Gutzwiller expression for the

spectral density [15]. Section VII introduces the dynamical ζ function [16–21]. The results of calculations of the approximate energy eigenvalues are reported for several quantization schemes, including unsmoothed [20, 21] and smoothed [22] versions of the Riemann-Siegel look-alike equation, the simple product form combined with the functional equation [6], and Bogomolny's approach based on a quantum Poincaré surface of section (PSOS) [23, 24]. The results are compared and discussed in the final section.

II. SOLUTION OF THE SCHRÖDINGER EQUATION

A complete description of the quantum particle in the wedge is provided by the eigenvalues and eigenfunctions of the two-dimensional Schrödinger equation, with the potential $V(x,y) = y$. (Units are chosen so that $m = \hbar = 1$.) Consistent with the hard reflections of the classical billiard by the walls of the wedge, the boundary conditions for the quantum system are that the wave function $\psi(x,y)$ goes to zero at the wedge boundary lines $x = 0$ and $y = (\cot\phi_0)x$. (In this section we shall denote the wedge angle by ϕ_0 instead of ϕ.)

After this work was completed we learned of the doctoral thesis by Wittek [25] in which an elegant way of solving the Schrödinger equation for the wedge billiard is described. Wittek expands $\psi(x,y)$ in products of Airy functions, one member of each product being designed to be zero along the tilted wall of the wedge. Imposing the boundary condition that $\psi(x,y) = 0$ at N points along the vertical wall leads to a determinantal equation for the energy eigenvalues. This appears to be a natural way of obtaining the energy eigenvalues and eigenfunctions of the wedge billiard. It enabled Wittek to calculate the first 250 eigenvalues as a function of the wedge angle to high accuracy.

Our method of solving the Schrödinger equation for the wedge billiard, while not as efficient as Wittek's, is nevertheless able to give highly accurate results. Introducing polar coordinates (ρ,ϕ), with the wedge boundaries at $\phi = 0$ and $\phi = \phi_0$, we look for solutions of the Schrödinger equation of the form

$$\psi(\rho,\phi) = \sum_{l,m} c_{lm} P_l(\rho)\Phi_m(\phi), \tag{1}$$

with

$$\Phi_m(\phi) = (2/\phi_0)^{1/2}\sin(m\pi\phi/\phi_0), \quad m = 1,2,\ldots,m_{\max}. \tag{2}$$

The functions $\Phi_m(\phi)$ clearly ensure that the boundary conditions are satisfied. We have chosen the radial functions to have the form

$$P_l(\rho) = [2/(\rho\rho_0)]^{1/2}\sin(l\pi\rho/\rho_0), \quad l = 1,2,\ldots,l_{\max}. \tag{3}$$

Here ρ_0 is effectively a radial cutoff distance, since this form forces the wave functions to be zero at $\rho = \rho_0$. Both the $\Phi_m(\phi)$ and the $P_l(\rho)$ (with the weighting function ρ) are orthonormal sets of functions.

With the above choice of basis functions, the calculation of the eigenvalues E_i and the eigenfunctions $\psi_i(\rho,\phi)$ proceeds in the usual way. It is a straightforward matter [26] to calculate the matrix elements of the Schrödinger operator in the basis $P_l(\rho)\Phi_m(\phi)$. The eigenvalues of the resulting Hamiltonian matrix have been calculated on a Cray computer using 4900 basis functions. The numerical accuracy of the solutions depends, of course, on how $l_{\max}$, $m_{\max}$, and the cutoff distance ρ_0 are chosen.

Let us suppose that, for a specified wedge angle ϕ_0, we wish to obtain accurate energy eigenvalues up to some maximum energy $E_{\max}$. A classical particle of energy $E_{\max}$ can rise in the potential $V(x,y) = y$ to the height $y = E_{\max}$. If the quantum eigenfunctions are to be accurately represented up to this height, it is clear that the value of ρ_0 must be at least as large as

$$\rho_0 \approx E_{\max}/\cos\phi_0. \tag{4}$$

Now the maximum value of the radial kinetic energy, which occurs when $l = l_{\max}$, is equal to $(1/2)(l_{\max}\pi/\rho_0)^2$. Equating this to $E_{\max}$ we obtain the following approximate criterion for choosing $l_{\max}$:

$$l_{\max} \approx \frac{\sqrt{2}}{\pi\cos\phi_0}E_{\max}^{3/2}. \tag{5}$$

Finally, assuming that the detail to be resolved in the angular direction is about the same as in the radial direction, we choose $m_{\max} = l_{\max}$.

As a test case let us consider the 45° wedge, or, equivalently, the odd-parity solutions of the symmetric 90° wedge. For this angle the Schrödinger equation separates into two one-dimensional equations, each having the potential $V(x) = x/\sqrt{2}$. It is known [27] that the semiclassical eigenvalues of the one-dimensional equation, given by the Einstein-Brillouin-Keller (EBK) quantization rule, are in excellent agreement with the exact eigenvalues, except for the lowest few eigenvalues. With the ten lowest eigenvalues corrected (given by the zeros of the Airy function) the EBK semiclassical results give an accurate standard with which to compare the matrix calculation. If we choose $l_{\max} = m_{\max} = 65$, the approximate equations above give $E_{\max} \approx 22$ and $\rho_0 \approx 31$. The Thomas-Fermi contribution to the spectral density, to be described in Sec. VI, gives an estimate of the mean number of energy eigenvalues less than E:

$$N_{\mathrm{TF}}(E) \approx \frac{\tan\phi}{12\pi\hbar^2}E^3. \tag{6}$$

With $E = E_{\max} = 22$ this gives $N_{\mathrm{TF}}(E_{\max}) \approx 280$. Thus, if we choose $l_{\max} = m_{\max} = 65$ and $\rho_0 = 31.5$, we can expect to find good numerical accuracy for the lowest 280 eigenvalues of the Hamiltonian matrix. Comparison of the energy eigenvalues of the 4225×4225 matrix with the semiclassical results shows this expectation to be true, although the last 20% of the eigenvalues cannot be relied upon to differ from the semiclassical values by less than one-third of the mean level spacing.

To determine the energy eigenvalues of the 49° wedge and the 60° wedge we chose $l_{\max} = m_{\max} = 70$. (Each calculation of the eigenvalues of the resulting 4900×4900

matrix took about 1.25 h on a Cray computer.) For the 49° wedge the above equations yield $E_{\max} \approx 22$ and $\rho_0 \approx 33$, while Eq. (6) gives $N_{\rm TF}(E_{\max}) \approx 317$. For the 60° wedge we find $E_{\max} \approx 18$ and $\rho_0 \approx 36$, while $N_{\rm TF}(E_{\max}) \approx 278$. Reducing these values of $N_{\rm TF}(E_{\max})$ by 20%, we are confident that the calculated energy eigenvalues are in error by less than one-third of the mean spacing between the levels, up to about the 250th level for the 49° wedge and the 220th level for the 60° wedge.

III. ENERGY LEVEL SPACINGS

Since we have obtained accurate values for the lowest 200 to 300 energy eigenvalues of the 49° wedge and the 60° wedge, it is of considerable interest to calculate the distribution of level spacings. In terms of the variable s defined below, it is expected that for the quantum analog of a classically integrable system, such as the 45° wedge, the level spacings have a Poisson distribution, $P(s) = e^{-s}$, as suggested by Berry and Tabor [28] for a generic system (not a harmonic oscillator). On the other hand, it has been found [29,30,10] that the quantum analogs of classical systems exhibiting hard chaos and having time reversal symmetry generally have a distribution of level spacings that is well represented by

$$P(s) = \frac{\pi}{2} s \exp(-\pi s^2/4). \tag{7}$$

First introduced by Wigner in connection with the distribution of energy level spacings in nuclei, this function describes the distribution of spacings obtained from the eigenvalues of real symmetric random matrices. In random matrix theory these matrices constitute the Gaussian orthogonal ensemble (GOE). Thus, it is of interest to see whether the energy eigenvalues of the 49° wedge and the 60° wedge exhibit GOE statistics.

The variable s in the above distributions is defined so as to make the mean spacing between levels equal to unity. The mean spacing $\langle \Delta E \rangle$ at energy E is given by the inverse of the Thomas-Fermi density of states, $d_{\rm TF}(E)$, discussed in detail in Sec. VI. Thus, $\langle \Delta E \rangle d_{\rm TF}(E) = 1$. If we define the variable s by

$$s = E d_{\rm TF}(E)/3, \tag{8}$$

then, since the leading term in $d_{\rm TF}(E)$ varies as E^2 [see Eq. (23)], it follows that, to a good approximation,

$$\Delta s = s_{j+1} - s_j \approx \frac{d}{dE}\left(\frac{E d_{\rm TF}(E)}{3}\right)_{E=E_j} \Delta E \approx \Delta E \; d_{\rm TF}(E_j), \tag{9}$$

where, in this equation, $\Delta E = E_{j+1} - E_j$. Averaging over a suitable set of levels on both sides leads to $\langle \Delta s \rangle \approx 1$, which is the desired result.

Figure 1 shows a histogram calculated from the first 5000 level spacings for the 45° wedge. For this integrable case, accurate values for the energy eigenvalues were calculated as outlined in the preceding section. As expected, the histogram is very well fitted by the Poisson distribution, shown as the dashed curve in the figure. A similar result has been obtained for the 45° wedge by Wittek [25]. In contrast to this case, Figs. 2 and 3 show histograms of the level spacings for the first 300 eigenvalues of the 49° wedge and the first 250 eigenvalues of the 60° wedge. The dashed curve in each figure is the Wigner distribution, Eq. (7). Although the number of levels is not large enough to give good statistics, it is clear in both cases that the spacings are well described by the GOE distribution. Compared with the integrable case, there are very few level spacings with small values of s, showing the "level repulsion" expected for these quantum analogs of classically chaotic systems. Wittek [25] has also found approximately GOE behavior for the energy level spacings of eleven different wedge angles between 47° and 67°.

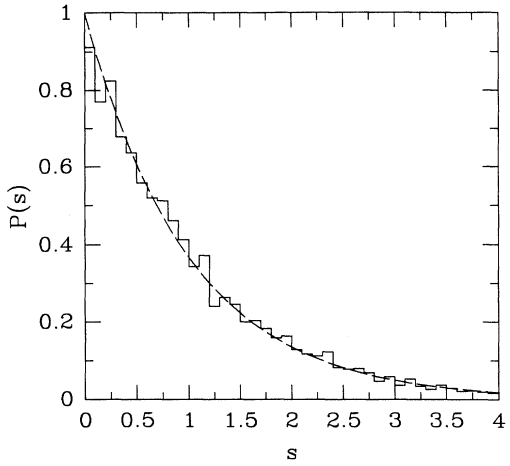

FIG. 1. Histogram of the level spacings for the 45° wedge, calculated from the lowest 5000 semiclasssical energy eigenvalues. The dashed curve is the Poisson distribution, $P(s) = e^{-s}$.

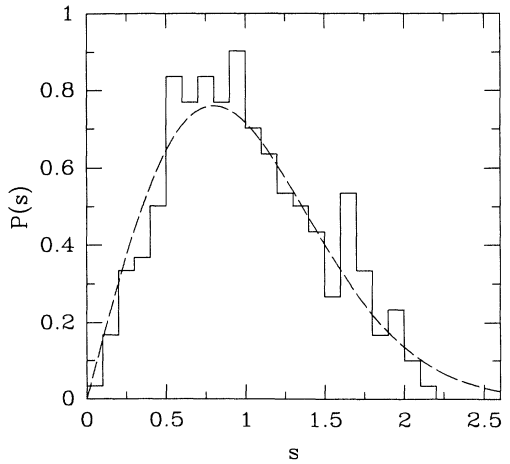

FIG. 2. Histogram of the level spacings for the 49° wedge, calculated from the lowest 300 eigenvalues of the Schrödinger equation. The dashed curve is the Wigner distribution, Eq. (7).

IV. THE GUTZWILLER TRACE FORMULA

Our starting point for studying the classical-quantum correspondence in a classically nonintegrable system is the Gutzwiller trace formula [1, 2]. Derived in the semiclassical approximation to quantum mechanics, the trace formula relates the energy eigenvalues of the quantum system to the periodic orbits of the classical system. For a classically chaotic system in which every periodic orbit is unstable, the form of the trace formula is

$$\sum_j \delta(E-E_j) = d_{\rm TF}(E) + \sum_\gamma \sum_{k=1}^{\infty} \frac{T_\gamma(E)}{\pi\hbar} \frac{\cos\{k[S_\gamma(E)/\hbar - \nu_\gamma\pi/2]\}}{\exp(ku_\gamma/2) - \sigma_\gamma^k \exp(-ku_\gamma/2)}, \tag{10}$$

where γ labels the primitive periodic orbits in the classical system, $T_\gamma(E)$ is the period of the orbit, $S_\gamma(E) = \oint \mathbf{p}\cdot d\mathbf{q}$ is the classical action, ν_γ is the Maslov index, u_γ is the stability exponent for one traversal of the orbit, and σ_γ is the sign of the trace of the monodromy matrix for one traversal of the orbit. Note that the two periodic orbits setting out in opposite directions from an arbitrary point on the orbit are counted as one contribution in the sum over γ. The sum over k counts multiple traversals of a given periodic orbit. $d_{\rm TF}(E)$ is the smoothly varying "Thomas-Fermi" or "Weyl" contribution to the density of states, which will be described in Sec. VI. Further details concerning Eq. (10) and its derivation may be found in Refs. [1, 2, 13, and 26].

The preceding paper gave a detailed description of the classical motion of the wedge billiard. It was shown that there is a simple scaling relation between a primitive periodic orbit at energy E and the corresponding orbit at any other energy, and that the topology of each orbit does not change as E varies. It was convenient to carry out all the calculations of the primitive periodic orbits at energy $E = 1$. Then the action and period at energy E are given by

$$S_\gamma(E) = E^{3/2} S_\gamma(1), \tag{11}$$

$$T_\gamma(E) = E^{1/2} T_\gamma(1) \tag{12}$$

while the Maslov index ν_γ, the stability exponent u_γ, and the sign of the trace of the monodromy matrix σ_γ are independent of the energy. Hence, for the wedge billiard with wedge angle ϕ greater than 45°, the trace formula becomes

$$\sum_j \delta(E-E_j) = d_{\rm TF}(E) + \sum_\gamma \sum_{k=1}^{\infty} \frac{E^{1/2}T_\gamma(1)}{\pi\hbar} \frac{\cos\{k\left[E^{3/2}S_\gamma(1)/\hbar - \nu_\gamma\pi/2\right]\}}{\exp(ku_\gamma/2) - \sigma_\gamma^k \exp(-ku_\gamma/2)}. \tag{13}$$

It was pointed out by Gutzwiller [16] that, in the case of a general nonintegrable system, the periodic orbit sum may not be absolutely convergent because the number of primitive periodic orbits with orbit length less than L appears to grow exponentially with L. An analysis of the periodic orbit sum has been carried out for homogeneous potentials by Eckhardt and Aurell [31] and for force-free billiards by Sieber and Steiner [32]. Allowing the energy E to be complex, they arrived at similar conditions guaranteeing absolute convergence of the sum. These have the form

$$\text{const} \times \text{Im}(E^\alpha) > \tau - \bar{\lambda}/2, \tag{14}$$

where τ is the topological entropy and $\bar{\lambda}$ is the mean Lyapunov exponent averaged over suitably long periodic orbits. [See Secs. V and VI of paper I for definitions of these quantities. Strictly speaking, in (14) τ should be defined through the number of periodic orbits with periods between T and $T+dT$ being given by $\exp(\tau T)/T$ as $T \to \infty$.] In the above inequality the exponent α is $1/2$ for force-free billiards and is equal to $1/\kappa + 1/2$ for a particle moving in a homogeneous potential of degree κ. (For the wedge billiard, $\kappa = 1$ and $\alpha = 3/2$.) Numerical studies of the convergence of the periodic orbit sum as a function of orbit length L reported by Sieber [13] for the hyperbola billiard led him to conclude that the sum is very likely *conditionally* convergent, and might even be *absolutely* convergent for real values of E.

Although the topological entropy cannot be defined for the wedge billiard because of the existence of infinite families of primitive periodic orbits having nearly the same action (or period), we showed in paper I that, by analogy, one can define a word length entropy τ_w. [Letting $N(n)$ denote the number of primitive periodic orbits of word length n, we defined τ_w through $N(n) \sim \exp(\tau_w n)$

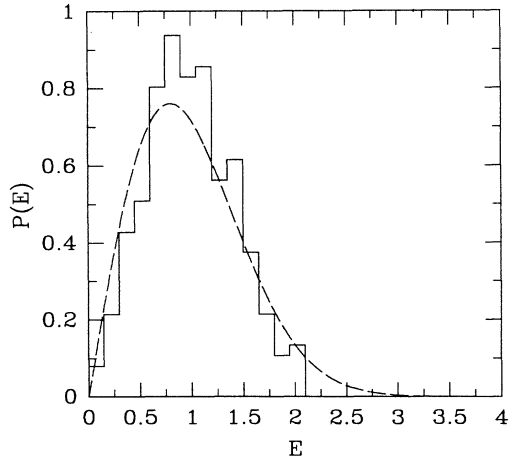

FIG. 3. Histogram of the level spacings for the 60° wedge, calculated from the lowest 250 eigenvalues of the Schrödinger equation. The dashed curve is the Wigner distribution, Eq. (7).

as $n \to \infty$.] This suggests that we analyze the convergence of the periodic orbit sum for the wedge billiard in terms of n.

First, we note that the convergence of the sum will not be affected if the factor involving the stability exponent in Eq. (13) is replaced by $\exp(-ku_\gamma/2)$. (Recall from paper I that, to a good approximation, the value of u_γ increases linearly with n.) Reverting from the cosines in Eq. (13) back to exponentials, we see that the convergence of the periodic orbit sum depends on

$$\sum_\gamma \sum_{k=1}^{\infty} \frac{E^{1/2} T_\gamma(1)}{\pi\hbar} \exp\{ ik[E^{3/2} S_\gamma(1)/\hbar - \nu_\gamma \pi/2] - ku_\gamma/2\}. \tag{15}$$

We now change the sum over γ to a sum over the word length n of the primitive periodic orbits, making use of the following results from paper I:

$$\bar{S}(n) \underset{n\to\infty}{\sim} a_s n, \tag{16}$$

$$\bar{\nu}(n) \underset{n\to\infty}{\sim} a_\nu n, \tag{17}$$

$$\bar{u}(n) \underset{n\to\infty}{\sim} a_u n, \tag{18}$$

where the constants a_s, a_ν, and a_u are the slopes of the appropriate straight lines in Figs. 10, 12, and 13 of paper I. Recalling that $T_\gamma(1) = (3/2)S_\gamma(1)$ and ignoring an overall constant factor, we write the double sum in Eq. (15) as being approximately equal to

$$\sum_{n=1}^{\infty}\sum_{k=1}^{\infty} N(n)\bar{S}(n) \exp\{ik[E^{3/2}\bar{S}(n)/\hbar - \bar{\nu}(n)\pi/2] - k\bar{u}(n)/2\}$$
$$= \sum_{n=1}^{\infty} \bar{S}(n) \sum_{k=1}^{\infty} \exp\{ikn[\mathrm{Re}(E^{3/2})a_s/\hbar - a_\nu\pi/2]\} \exp\{n[\tau_w - k\,\mathrm{Im}(E^{3/2})a_s/\hbar - ka_u/2]\}. \tag{19}$$

Clearly, absolute convergence is assured if

$$k\,\mathrm{Im}(E^{3/2})a_s + ka_u/2 - \tau_w > 0 \qquad \text{for all } k \geq 1. \tag{20}$$

When E is real, the key condition is (since a_u is positive)

$$a_u/2 - \tau_w > 0 \qquad (E \text{ real}). \tag{21}$$

The slopes of the straight lines in Figs. 9 and 13 of paper I have the following values: for the 49° wedge, $a_u = 0.474$, $\tau_w = 0.368$, giving $a_u/2 - \tau_w = -0.131$; for the 60° wedge, $a_u = 0.635$, $\tau_w = 0.510$, giving $a_u/2 - \tau_w = -0.193$. Thus, in neither case is the criterion for absolute convergence satisfied for real E.

Despite this failure to converge absolutely, the periodic orbit sum may, however, be conditionally convergent for real E, since the terms in the double sum in Eq. (13) enter with either sign, allowing a systematic cancellation to occur. Of course, the answer obtained from a given computation will depend on how the summations are truncated. Nevertheless, it is interesting to calculate the right-hand side of Eq. (13) as a function of energy using a restricted number of primitive periodic orbits, and compare the resulting peaks with the eigenvalues of the Schrödinger equation. [Since the Thomas-Fermi term $d_{\mathrm{TF}}(E)$ is slowly varying it has been omitted in the following.]

Such a calculation for the 49° wedge is shown in Fig. 4. The sum over γ included 1048 primitive periodic orbits having actions less than 12.0 and word lengths ≤ 19. The sum over k was taken up to $k = 9$, by which point the contributions were always negligible. It should be noted that the abscissa was chosen to be $Ed_{\mathrm{TF}}(E)/3$ rather than E since this has the effect of making the mean spacing between the energy levels equal to unity. [See Eq. (9).] From a careful examination of the figure one sees that peaks are situated close to the positions of the first 11 eigenvalues, although at the fourth and seventh eigenvalues there occur two very narrow peaks of nearly the same height. Spanning the twelfth and thirteenth eigenvalues are three small peaks. Above that, some peaks occur in the right positions, but others do not. Moreover, several pairs of close eigenvalues are not resolved by the periodic orbit sum. Overall, the agreement between the classical and quantum calculations is not very satisfactory. It should be added that if only 271 primitive periodic orbits are included in the sum, the agreement is almost as good as in Fig. 4, although some features are slightly less well resolved.

A similar calculation for the 60° wedge containing 1621 primitive periodic orbits with actions less than 19.4 and

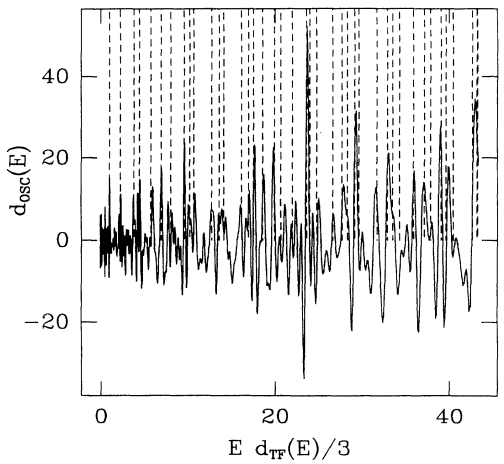

FIG. 4. Comparison of the exact eigenvalues of the Schrödinger equation for the 49° wedge (dashed lines) with the results of the Gutzwiller periodic orbit sum (solid line). The sum included 1048 primitive periodic orbits with actions less than 12.0 and word lengths $n \leq 19$.

word lengths ≤ 15 (plus some of length 16) is shown in Fig. 5. In this case the periodic orbit sum accurately determines the positions of the first 20 eigenvalues. Beyond that point, the 21st peak is small and pairs of close eigenvalues are not well resolved, although the resolution of these higher energy peaks is distinctly better than when only 257 primitive periodic orbits are included in the sum. It is evident that the periodic orbit sum is much more successful for the 60° wedge than for the 49° wedge. This may be related to the fact that there is considerably less pruning of orbits for the 60° wedge.

Why is the agreement between the classical and the quantum calculations not better than it is shown to be in Figs. 4 and 5? One reason is, undoubtedly, the truncation of the sum over primitive periodic orbits and the fact that if the sum is convergent at all, it is only conditionally convergent. Another reason is the existence of families of primitive periodic orbits with very nearly the same action. This feature will be analyzed in the next section.

V. FAMILIES OF PRIMITIVE PERIODIC ORBITS

It was shown in paper I that when the wedge angle is greater than 45°, there occur many families of primitive periodic orbits having very nearly the same action. Since the members of a given family become closer and closer together in the phase space as the word length n increases, there may well come a point at which there is a failure of the stationary-phase approximation used in deriving the Gutzwiller trace formula. The stationary-phase approximation requires that when variations in the paths are made away from a primitive periodic orbit, the accompanying changes in the action are large compared to $\hbar$, thus giving rise to an efficient cancellation of the contributions from all the paths for which the action is not an extremum.

Let us examine the situation in more detail. For a particular family of primitive periodic orbits, the orbit of

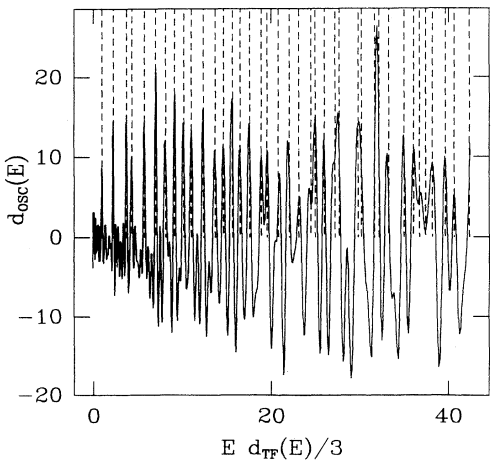

FIG. 5. Comparison of the exact eigenvalues of the Schrödinger equation for the 60° wedge (dashed lines) with the results of the Gutzwiller periodic orbit sum (solid line). The sum included 1621 primitive periodic orbits with actions less than 19.4 and word lengths $n \leq 15$, plus some with $n = 16$.

word length n makes a series of T bounces up the tilted wall until it reaches its highest reflection point. We shall denote the radial distance of the reflection point farthest from the wedge vertex by ρ_n. [As $n \to \infty$, this highest reflection point approaches the point $x = \tan\phi$, $y = 1$, and ρ_n approaches $(1+\tan^2\phi)^{1/2}$.] The action S_n corresponding to the primitive periodic orbit of word length n is an extremum with regard to small variations of the path. Consequently, if a change $\Delta\rho$ is made from ρ_n as the starting point for a varied path in the phase space, and if the new path can be made to close upon itself (by varying the component of momentum perpendicular to the primitive periodic orbit n), then the first order change in the action, δS, will be zero, but the second order change, $\delta^2 S$, will be nonzero (positive or negative). Using quadruple precision arithmetic we have verified that the change in the action resulting from a change $\Delta\rho$ in the initial conditions *is* actually proportional to $(\Delta\rho)^2$.

Now the key factor entering the Green's function $\tilde{G}(q'', q', E)$ in Gutzwiller's derivation of the trace formula [1] has the form $\exp[i\Xi(\delta q_2)^2/\hbar]$, where, as in paper I,

$$\Xi = \frac{1}{2}\left(\frac{\partial^2 S}{\partial q_2' \partial q_2'} + 2\frac{\partial^2 S}{\partial q_2' \partial q_2''} + \frac{\partial^2 S}{\partial q_2'' \partial q_2''}\right). \tag{22}$$

Here, as in Gutzwiller's original paper, q_2 is the coordinate in a direction perpendicular to the primitive periodic orbit, while q_2' and q_2'' are the initial and final positions. The partial derivatives in Ξ are evaluated at the starting point of the primitive periodic orbit, which we take to be the highest reflection point on the tilted wall. From the expression above it is clear that the Fresnel integral resulting from the integration over δq_2 can be performed cleanly when Ξ times the square of half the range of integration over δq_2 is much larger than $\hbar$. However, if the q_2 separation between orbits n and $n+1$ is sufficiently small, the integrands of the Fresnel integrals for these orbits overlap and the stationary-phase approximation can no longer be carried out in the customary manner.

Figure 6 shows a plot of $\ln[\Xi(\Delta\rho)^2/\hbar]$ against $\ln m$, where $\Delta\rho = \rho_{m+1} - \rho_m$ is the difference between the highest reflection points on the tilted wall for the primitive periodic orbits corresponding to $m+1$ and m of the family $T^m VVTTVV$ of the 49° wedge. Even for the first point of this figure, which corresponds to the difference between the primitive periodic orbits $T^4VVTTVV$ and $T^3VVTTVV$, the value of $\Xi(\Delta\rho)^2$ is only 0.3 in units of $\hbar$. By the time $m = 41$, the last point of the figure, it has fallen to 0.003. Figure 7 shows a similar plot for the family $T^m VVV$ of the 60° wedge. In this case $\Xi(\Delta\rho)^2$ decreases from about 0.39 for $m = 5$ to 0.11 for $m = 44$.

The above calculations, which were performed in units in which $\hbar = 1$, show clearly that the primitive periodic orbits in a given family become very close together and are not separated by an appreciable barrier due to Ξ, defined in Eq. (22). This means that in the derivation of the Gutzwiller trace formula, the stationary-phase approximation will become invalid at some point as m increases, although it is not clear exactly where it will fail. Note that even if $\hbar$ were to have a much smaller value, in the

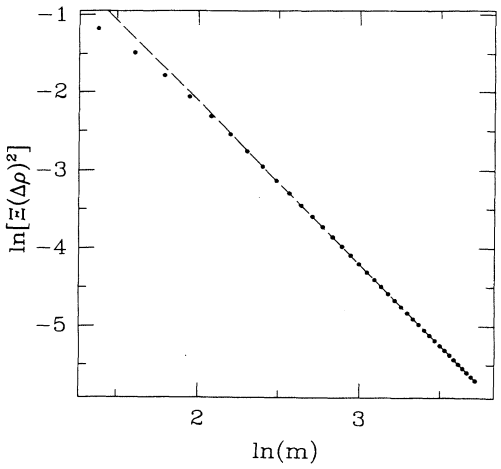

FIG. 6. Plot of $\ln[\Xi(\Delta\rho)^2]$ against $\ln m$ for members of the family $T^mVVTTVV$ of the 49° wedge, for $m = 4$ to 41. Ξ and $\Delta\rho$ are defined in the text. The dashed line corresponds to $\Xi(\Delta\rho)^2 = 7.96/m^{2.09}$.

spirit of taking the semiclassical limit, the stationary-phase approximation would still be in trouble at some point in each family of primitive periodic orbits of the type we are considering.

Finally, we note that the periodic orbit sums in Figs. 4 and 5 were cut off at word lengths of 19 for the 49° wedge and 15 or 16 for the 60° wedge. The fact that the positions of the first 10 or 20 peaks are in reasonably good agreement with the quantum energy eigenvalues may be an indication that the truncated contributions from these infinite families are not badly in error. As Tanner and Wintgen [6] have observed for the anisotropic Kepler problem, it is possible that a grand cancellation occurs among the members of each family with longer word lengths.

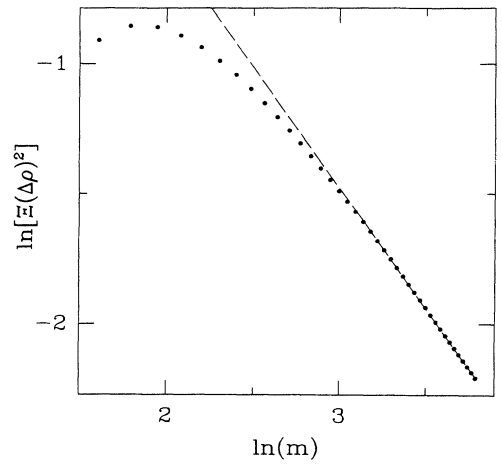

FIG. 7. Plot of $\ln[\Xi(\Delta\rho)^2]$ against $\ln m$ for members of the family T^mVVV of the 60° wedge, for $m = 5$ to 44. Ξ and $\Delta\rho$ are defined in the text. The dashed line corresponds to $\Xi(\Delta\rho)^2 = 3.67/m^{0.93}$.

VI. THE THOMAS-FERMI TERM AND STAIRCASE QUANTIZATION

In this section we study how to use the spectral staircase function $N(E)$ to calculate approximate quantum energy eigenvalues on the basis of the periodic orbits of the classical system. Defined as the number of energy eigenvalues less than or equal to E, $N(E)$ for the wedge billiard is readily obtained by integrating Eq. (13) from 0 to E. In order to do this we require an accurate representation of the Thomas-Fermi contribution $d_{\rm TF}(E)$.

We have calculated the Thomas-Fermi contribution by a method similar to that described by Kac [33] in a well-known article entitled "Can you hear the shape of a drum?" The calculation starts from the semiclassical or WKB expression for the time-dependent propagator for a particle in the potential $V(x,y) = y$. We then calculate an approximation to the partition function $\sum \exp(-sE_j)$, which is the Laplace transform of the spectral density $\sum \delta(E - E_j)$, by integrating the short-time propagator over all space, putting $s = it$. The following result is obtained after taking the inverse Laplace transform:

$$d_{\rm TF}(E) = \frac{\tan\phi}{4\pi\hbar^2}E^2 - \frac{(1+\sec\phi)}{2\sqrt{2\pi}\hbar}E^{1/2} + \frac{1}{6}\delta(E). \qquad (23)$$

The first term on the right-hand side comes from integrating the propagator over the domain of the wedge, while the second term is a correction from (short) paths in which the particle is reflected from one of the walls of the wedge. The third term has not been derived by us, but is suggested by a result of Pleijel quoted by Kac [33]. (Its ultimate justification is that it is essential in giving an excellent fit to the exact staircase function over a broad range of energies, as will be described below.) It should be added that the method we have used to calculate $d_{\rm TF}(E)$ is similar to that employed by Steiner and Trillenberg [34] to calculate the partition function for an unbounded force-free quantum billiard. Further details of our calculation may be found in the Ph.D. thesis by Szeredi [26].

The result of integrating the left-hand side of Eq. (13) is the exact staircase function for the quantum system:

$$N(E) = \sum_{j=1}^{\infty} \theta(E - E_j), \qquad (24)$$

where, as usual, $\theta(x)$ is 0 for $x < 0$ and 1 for $x > 0$. Integrating the right-hand side of Eq. (13) leads to a semiclassical approximation to the staircase function having the form

$$N_{\rm sc}(E) = N_{\rm TF}(E) + N_{\rm osc}(E). \qquad (25)$$

From Eq. (23) the Thomas-Fermi contribution is found to be

$$N_{\rm TF}(E) = \frac{\tan\phi}{12\pi\hbar^2}E^3 - \frac{(1+\sec\phi)}{3\sqrt{2\pi}\hbar}E^{3/2} + \frac{1}{6}. \qquad (26)$$

The expression for the oscillating part, $N_{\rm osc}(E)$, which is readily obtained from Eq. (13), will not be given explicitly here.

Ignoring $N_{\rm osc}(E)$ for the moment, we have found that $N_{\rm TF}(E)$ given by Eq. (26) follows the exact staircase function very closely for the first 380 eigenvalues of the 49° wedge and for the first 280 eigenvalues of the 60° wedge—well beyond the points at which the eigenvalues are no longer accurate to within one-third of the mean spacing between the levels.

To formulate a quantization rule capable of giving reasonably accurate values for the energy eigenvalues, it is necessary to add $N_{\rm osc}(E)$ to the Thomas-Fermi contribution. Figure 8, for the 60° wedge, compares the exact staircase function $N(E)$ with the result of calculating $N_{\rm sc}(E)$ using 1621 primitive periodic orbits having actions ≤ 19.4 and word lengths ≤ 15, plus some of length 16. (A calculation with 257 primitive periodic orbits gave almost identical results.) The figure covers the range of the lowest 18 eigenvalues, the abscissa being chosen to be $Ed_{\rm TF}(E)/3$ in order to make the mean spacing between levels equal to unity. One sees that $N_{\rm osc}(E)$ attempts to chisel out the steps from the Thomas-Fermi "background," indicated by the dashed curve in Fig. 8. However, it is not very successful in doing this, particularly for the wider steps in the figure. For the 49° wedge, $N_{\rm osc}(E)$, computed with 271 primitive periodic orbits having actions ≤ 12, is even less successful in approximating the exact staircase.

A staircase quantization rule can now be stated: the jth eigenvalue of the quantum system is given by

$$N_{\rm TF}(E_j) + N_{\rm osc}(E_j) = j - 1/2, \qquad j = 1, 2, \ldots . \tag{27}$$

This rule, which has been proposed by Aurich and Steiner [15], works very well for most of the eigenvalues of the 60° wedge. Occasionally, however, when there is more than one solution to the above equation, it needs to be supplemented by requiring that one choose the solution closest to $E_j^{\rm TF}$ satisfying $N_{\rm TF}(E_j^{\rm TF}) = j - 1/2$. This is essential in the case of the 49° wedge if one is to avoid ambiguity in some of the first 20 eigenvalues.

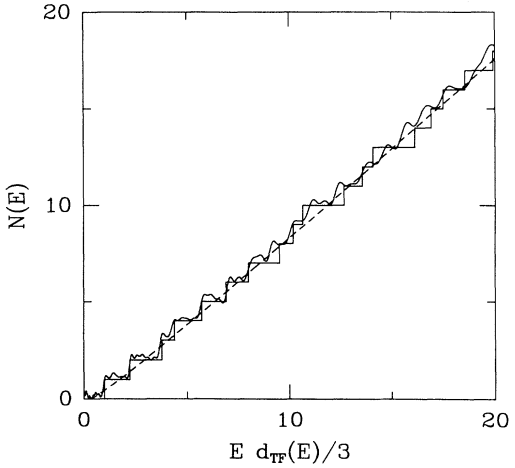

FIG. 8. Plot of the staircase function $N(E)$ against $Ed_{\rm TF}(E)/3$ for the 60° wedge. The stepped curve was calculated from the first 18 eigenvalues of the Schrödinger equation. The dashed curve is the Thomas-Fermi function $N_{\rm TF}(E)$ given by Eq. (26). The oscillating solid curve is the semiclassical approximation $N_{\rm sc}(E)$ which includes the contribution from the periodic orbit sum.

VII. THE DYNAMICAL ζ FUNCTION

A different approach to calculating approximate semiclassical energy eigenvalues from a knowledge of the periodic orbits of the classical system is based on the dynamical ζ function. First introduced in this context by Gutzwiller [16] and discussed in pioneering papers by Berry [17] and Voros [19], the dynamical ζ function consists of an infinite product over the primitive periodic orbits of the system. The current interest in studying various approximations to the dynamical ζ function for classically chaotic systems stems from the possibility that they may have better convergence properties than the Gutzwiller trace formula, which, as we have seen in Sec. IV, is at best conditionally convergent.

A. Formal relations

The derivation of the dynamical ζ function, for a system in which all the primitive periodic orbits are unstable, starts from the expression [1, 19]

$$\lim_{\varepsilon\to 0}\sum_j \frac{1}{E + i\varepsilon - E_j} = g_{\rm TF}(E) + \sum_\gamma \sum_{k=1}^{\infty} \frac{T_\gamma(E)}{i\hbar} \frac{\exp\{ik[S_\gamma(E)/\hbar - \nu_\gamma\pi/2]\}}{\exp(ku_\gamma/2) - \sigma_\gamma^k \exp(-ku_\gamma/2)}, \tag{28}$$

where [24]

$$g_{\rm TF}(E) = \lim_{\varepsilon\to 0}\int_{-\infty}^{\infty} \frac{d_{\rm TF}(E')dE'}{E + i\varepsilon - E'}. \tag{29}$$

Note that Eq. (10) is obtained at once from Eq. (28) by taking $(-1/\pi)$ times the imaginary part of both sides.

Now the left-hand side of Eq. (28) can be put in the form

$$\lim_{\varepsilon\to 0}\frac{d}{dE}\ln[\Pi_j(E + i\varepsilon - E_j)] = \frac{d}{dE}\ln[\Pi_j(E - E_j)]. \tag{30}$$

After some straightforward algebraic manipulations [19, 13], and interchanging the order of the limit and the integration in the Thomas-Fermi term, the right-hand side can be expressed in the form

$$\frac{d}{dE}\{\ln\exp[-i\pi N_{\rm TF}(E)]\} + \frac{d}{dE}\ln Z(E), \tag{31}$$

where $Z(E)$ is the dynamical ζ function,

$$Z(E) = \prod_\gamma \prod_{n=0}^{\infty}\{1 - \sigma_\gamma \exp[\, iS_\gamma(E)/\hbar - i\nu_\gamma\pi/2 - (n + 1/2)u_\gamma]\}. \tag{32}$$

By integrating over E from 0 to E and exponentiating the result one obtains

$$\prod_j (1 - E/E_j) = \exp[-i\pi N_{\rm TF}(E)]Z(E)/Z(0). \quad (33)$$

From the left-hand side of this relation it is clear that the function on the right-hand side has zeros at the energy eigenvalues E_j. Furthermore, since for real E the left-hand side is real, it follows that $Z^*(0)\exp[-i\pi N_{\rm TF}(E)]Z(E)$ is also real. This is consistent with the fact that $\exp[-i\pi N_{\rm TF}(E)]Z(E)$ is real when E is real, a result that follows from the well known "functional equation"

$$\exp[-i\pi N_{\rm TF}(E)]Z(E) = \exp[i\pi N_{\rm TF}(E)]Z^*(E). \quad (34)$$

[Putting $E = 0$ and $N_{\rm TF}(0) = 0$ in this relation shows that $Z(0)$ is real.] This has been proved for the dynamical ζ function of a free billiard by Sieber and Steiner [12]. We have adapted their proof to show that it also holds for the wedge billiard, which has a different scaling relation for the actions.

We note that all the above relations are valid only to the extent that the original Gutzwiller relation, Eq. (28) is valid—recall its semiclassical origin in the stationary-phase approximation—and provided none of the sums in Eq. (28) or the infinite products in Eqs. (32) and (33) are truncated. When $Z(E)$ is truncated in some fashion, the right-hand side of Eq. (33) can no longer be assumed to be real [21] for real E. Nevertheless, in the following subsections we shall often incorporate the functional equation into a quantization scheme by assuming that the approximate semiclassical energy eigenvalues are given by the equation

$$\mathrm{Re}\{\exp[-i\pi N_{\rm TF}(E)]Z(E)\} = 0, \quad (35)$$

with $Z(E)$ calculated as either a truncated Euler product or a truncated Dirichlet series.

B. Calculations with $Z(E)$ as a truncated product

The simplest quantization rule based on the preceding theory comes from the observation that the right-hand side of Eq. (33) vanishes at the zeros of the left-hand side if $Z(E_j) = 0$. Since in an actual calculation one must truncate the ζ product at some point, its zeros will occur at complex rather than real values of E. However, these approximate zeros of $Z(E)$ may be situated close to the real axis. If their imaginary parts are small, it is plausible that the truncated $|Z(E)|$, evaluated as a function of E, will display minima near the exact eigenvalues of the Schrödinger equation.

In Fig. 9 we show the results of calculating $|Z(E)|$ as a function of the real variable E for the 60° wedge. The calculation was performed using 1621 primitive periodic orbits with actions ≤ 19.4 and word lengths ≤ 15 plus some of length 16. For every primitive periodic orbit the product over n in Eq. (32) was carried as far as $n = 9$. As in the earlier calculations, the abscissa was chosen to be $Ed_{\rm TF}(E)/3$ in order to make the mean spacing equal to unity. The triangles in the figure show the positions of the exact eigenvalues of the Schrödinger equation. Ignoring the first minimum at $E = 0$, we see that the first 18 minima in $|Z(E)|$ are very close to the exact eigenvalues. Beyond that point, the 19th and the 21st minima are rather far from the energy axis, and subsequent pairs of close eigenvalues are not resolved. Nevertheless, it is interesting that a quantization rule base on picking off the minima of $|Z(E)|$, subject to the condition that $|Z(E)| < 1$, is quite successful for the first 18 eigenvalues.

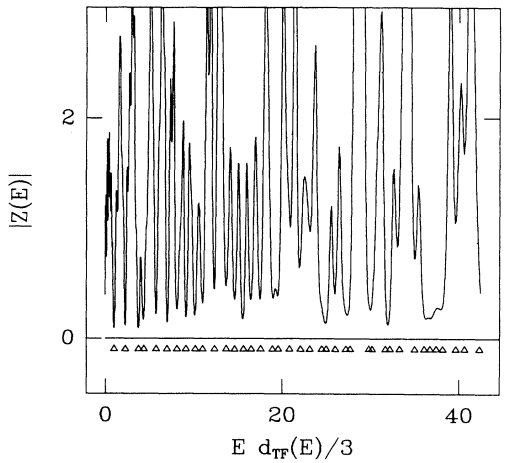

FIG. 9. The absolute value of the ζ product, Eq. (32), plotted against $Ed_{\rm TF}(E)/3$ for the 60° wedge. The calculation was carried out using 1621 primitive periodic orbits with actions ≤ 19.4 and word lengths ≤ 15, plus some of length 16. The triangles show the positions of the exact energy eigenvalues of the Schrödinger equation.

Similar calculations of $|Z(E)|$ as a function of energy have been carried out for the 49° wedge using 1048 primitive periodic orbits having word length ≤ 19. The result is the solid curve in Fig. 10. One can see that there are two minima instead of one near the fourth energy eigenvalue, and also two "high" minima in the vicinity of the seventh energy eigenvalue. Clearly, the results are less satisfactory than in the case of the 60° wedge, even for the lowest energy eigenvalues.

It is natural to ask whether better results are obtained if use is made of the functional equation. Accordingly, we have calculated the left-hand side of Eq. (35) as a function of energy for the 49° wedge, with $Z(E)$ calculated as described in the preceding paragraph. The result is the solid curve in Fig. 11. The black dots on the energy axis indicate the positions of the exact eigenvalues of the Schrödinger equation, and, as in the previous figures, the abscissa was chosen to be $Ed_{\rm TF}(E)/3$ in order to make the mean spacing between the energy levels approximately equal to unity. It may be seen that the zeros of the solid curve are close to the exact eigenvalues for the first 18 eigenvalues, and remain fairly close up to the right side of the figure. The solid curve even manages to predict correctly that there are two very closely spaced zeros near the 40th and 41st eigenvalues (at the far right of the figure). The solid curve does not miss any zeros or introduce any spurious zeros over the energy range encompassing the first 100 energy eigenvalues.

For the 60° wedge there is a similar success (not shown here), with no missing zeros or spurious zeros. Thus we have found that the simple ζ product, Eq. (32), taken over about a thousand primitive periodic orbits, and combined with the functional equation as in Eq. (35), gives very good results for the approximate energy eigenvalues.

C. The pseudo-orbit expansion

By analogy with the Riemann ζ function, the dynamical ζ function of Eq. (32) can be expressed as a Dirichlet series having the form [20, 21, 12],

$$Z(E) = 1 + \sum_{n=1}^{\infty} A_n \exp[iS_n(E)/\hbar], \tag{36}$$

where,

$$S_n(E) = \sum_{i=1}^{\infty} m_i S_{\gamma_i}(E), \tag{37}$$

and the m_i are positive integers. The coefficients A_n have been derived by Berry and Keating [20] and by Sieber and Steiner [12]:

$$A_n = \prod_i \left(\frac{(-1)^{m_i} \sigma_{\gamma_i}^{m_i(m_i-1)/2} \exp[-im_i\nu_{\gamma_i}\pi/2 - m_i(m_i-1)u_{\gamma_i}/4]}{\prod_{j=1}^{m_i} [\exp(ju_{\gamma_i}/2) - \sigma_{\gamma_i}^{j} \exp(-ju_{\gamma_i}/2)]} \right). \tag{38}$$

Here n labels the *pseudo-orbits*, each pseudo-orbit being made up of a unique linear combination of primitive periodic orbits in which the particular orbit γ_i occurs m_i times. The quantity $S_n(E)$ in Eq. (36) is the *pseudo-action* for the pseudo-orbit specified by the integers m_i.

The pseudo-orbit expansion for $Z(E)$, truncated at some point, provides a different way of approximating the dynamical ζ function when one has a finite number of primitive periodic orbits. A better form of this expansion is the Riemann-Siegel look-alike equation [20, 21] and its refinement to include smoothing of the cutoff [22], which will be the subject of the next subsection. However, it is of interest to look at the results obtained from a simple truncation of the series.

In general, the pseudo-orbits can be arranged in order of increasing action [$S_n(E) \leq S_{n+1}(E)$ for all $n \geq 1$], or in order of increasing word length. For the wedge billiard, the infinite families of primitive periodic orbits having nearly the same action make the former scheme impracticable. We have therefore truncated the series at a specified word length, denoted by N. This means that every pseudo-orbit contributing to the sum in Eq. (36) is made up of primitive periodic orbits γ_i such that the sum of their word lengths (allowing for m_i repetitions of γ_i) does not exceed N. As in the preceding section, the quantization rule is simply that $Z(E_j) = 0$, and,

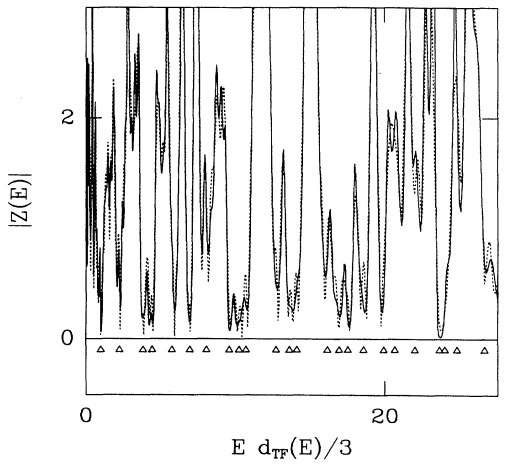

FIG. 10. Comparison of the product form of $|Z(E)|$ with the results of the pseudo-orbit expansion for $|Z(E)|$ for the 49° wedge. Solid curve: the product form, Eq. (32), calculated with 1048 primitive periodic orbits with word length $\leq$ 19. Dotted curve: the pseudo-orbit expansion containing 26706 pseudo-orbits with word length $\leq$ 19. The triangles show the positions of the exact energy eigenvalues of the Schrödinger equation.

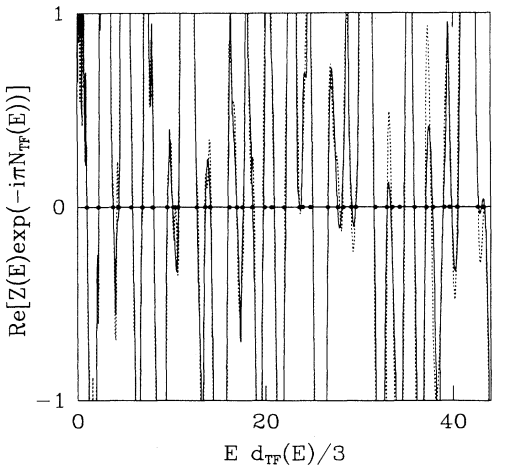

FIG. 11. The results of calculations for the 49° wedge employing the functional equation. Both curves show the left-hand side of Eq. (35) as a function of energy. The solid curve was calculated from the ζ product, Eq. (32), with 1048 primitive periodic orbits having word length $\leq$ 19. The dotted curve was calculated using a pseudo-orbit expansion consisting of 26706 pseudo-orbits with word length $\leq$ 19. The positions of the exact energy eigenvalues are indicated by the solid circles.

because of the truncation, the zeros E_j are expected to be complex with small imaginary parts.

Instead of searching for the complex zeros of $Z(E)$, we have calculated $|Z(E)|$ for real E as a function of the energy. The dotted curve in Fig. 10 is the result for the 49° wedge of the pseudo-orbit expansion with $N = 19$, there being 26706 pseudo-orbits contributing up to this word length. It is noticeable that the minima of the pseudo-orbit calculation are sharper and deeper than those of the simple product form (the solid curve in the figure). However, there are many more minima of the pseudo-orbit calculation than there are eigenvalues of the Schrödinger equation, the positions of which are indicated by the triangles in the figure. For example, there are two minima near the seventh eigenvalue, four minima in the vicinity of the next three eigenvalues, four minima near the next three eigenvalues, and so on. Thus, it appears that for the 49° wedge the pseudo-orbit expansion does not yield an improvement over the straight product form.

In view of this lack of success, one is led to examine the convergence of the pseudo-orbit expansion. Because it does not make sense to label the pseudo-orbits in order of increasing pseudoactions, we break up the sum in Eq. (36) into sets of pseudo-orbits of given word length n_w. A numerical analysis of all the 26706 pseudo-orbits of the 49° wedge with $n_w \leq 19$ shows that the pseudoactions of word length n_w have a mean value proportional to n_w, the proportionality relation being excellent over the range $11 \leq n_w \leq 19$. Since the actions at energy E are proportional to $E^{3/2}$, we add an imaginary part to $E^{3/2}$ and examine the convergence of

$$\sum_{n_w=1}^{\infty}\left\{\sum_p A_p \exp[iS_p(1)\mathrm{Re}(E^{3/2})/\hbar] \times \exp[-S_p(1)\mathrm{Im}(E^{3/2})/\hbar]\right\}, \tag{39}$$

where the sum over p includes all the pseudo-orbits of word length n_w. We now replace the pseudoactions at word length n_w by their average value $(\alpha_s\hbar)n_w$, where α_s is a constant (approximately equal to 0.847 for the 49° wedge). The double summation above is now approximately equal to

$$\sum_{n_w=1}^{\infty} \exp[in_w\alpha_s\mathrm{Re}(E^{3/2})]\exp[-n_w\alpha_s\mathrm{Im}(E^{3/2})]\sum_p A_p. \tag{40}$$

Adapting the analysis of Matthies and Steiner [35] to the present situation, we define, for each word length n_w, the quantities

$$\sigma_a(n_w) = \frac{1}{n_w\alpha_s}\ln\left(\sum_p |A_p|\right), \quad \sigma_a = \lim_{n_w\to\infty}\sigma_a(n_w), \tag{41}$$

$$\sigma_c(n_w) = \frac{1}{n_w\alpha_s}\ln\left|\sum_p A_p\right|, \quad \sigma_c = \lim_{n_w\to\infty}\sigma_c(n_w), \tag{42}$$

the sums over p including only the pseudo-orbits of word length n_w. It is now easy to see that if the limits σ_a and σ_c exist, the above series is absolutely convergent if $\mathrm{Im}(E^{3/2}) > \sigma_a$ and is conditionally convergent if $\mathrm{Im}(E^{3/2}) > \sigma_c$. The results of calculations of $\sigma_a(n_w)$ and $\sigma_c(n_w)$ as a function of n_w for the 26706 pseudo-orbits of the 49° wedge are shown in Fig. 12. While $\sigma_a(n_w)$ appears to approach a limit in the range of n_w covered by the calculations, $\sigma_c(n_w)$ does not. Since $\sigma_a \approx 0.24$, we conclude that the pseudo-orbit expansion does not converge absolutely for real E. Nevertheless, there is an indication that the series may be conditionally convergent for real E since $\sigma_c(n_w)$ remains negative over the range of n_w in the figure.

What happens if the truncated pseudo-orbit expansion is combined with the functional equation? The dotted curve in Fig. 11 shows the left-hand side of Eq. (35) calculated as a function of energy taking into account 26706 pseudo-orbits of the 49° wedge having word length ≤ 19. The agreement between the zeros of this curve and the exact energy eigenvalues is not as good as was obtained from the product form using a comparable truncation. In fact, if the scale is expanded one sees that the dotted curve puts two extra zeros near the fourth eigenvalue and two more extra zeros between the ninth and tenth eigenvalues. At higher energies than those shown in the figure, the pseudo-orbit expansion misses some zeros completely (in pairs). A similar calculation carried out by Sieber and Steiner [12] for the hyperbola billiard using 59370 pseudo-orbits appears to be of somewhat better accuracy, although it misses completely the 30th and 31st eigenvalues.

It should be mentioned that results of pseudo-orbit expansions for the 60° wedge are not presented here because of the existence, at this special angle, of numerous "vertex orbits"—primitive periodic orbits in which the billiard goes directly into the vertex of the wedge. The problem posed by the vertex orbits (described in some detail in paper I) is that they are not characterized by unique sequences of T's and V's. This difficulty disappears at wedge angles of, for example, 59.9° and 60.1°, since for these angles all the primitive periodic orbits are uniquely characterized. It would be interesting to carry

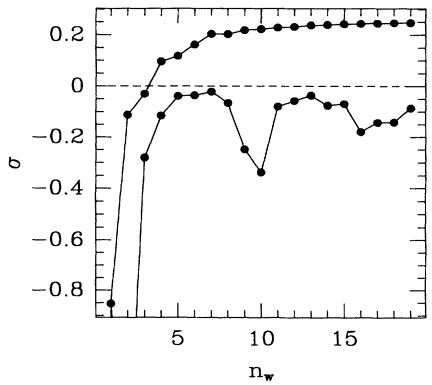

FIG. 12. Calculations for the 49° wedge of $\sigma_a(n_w)$ and $\sigma_c(n_w)$, defined in Eq. (41) and Eq. (42), as a function of n_w. The upper curve is $\sigma_a(n_w)$, the lower curve $\sigma_c(n_w)$.

out calculations for these two wedge angles and compare the results, but this has not been done so far.

D. The Riemann-Siegel look-alike equation

The unknown effect of sharply truncating the pseudo-orbit expansion is neatly avoided by the Riemann-Siegel look-alike equation. Keating [21] has shown that when $Z(E)$, in the form of Eqs. (36)–(38), is required to satisfy the functional equation, Eq. (34), the contributions to the sum at energy E from pseudo-orbits with periods greater than $\pi\hbar d_{\rm TF}(E)$ are related to the contributions from those with periods less than $\pi\hbar d_{\rm TF}(E)$. As a result, the approximate energy eigenvalues are given by the roots of the equation,

$$\mathrm{Re}\left\{1+\sum_{\substack{n\\(T_n\le T_{\rm RS})}} A_n \exp[iS_n(E)/\hbar - i\pi N_{\rm TF}(E)]\right\}=0, \tag{43}$$

which is known as the Riemann-Siegel look-alike equation [20,21]. In this equation, the sum over pseudo-orbits n is subject to the requirement that the period of the nth pseudo-orbit satisfies

$$T_n(E) \le T_{\rm RS} \equiv \pi\hbar d_{\rm TF}(E). \tag{44}$$

In a more recent paper, Berry and Keating [22] have reexamined and extended the theory of the dynamical ζ function in analogy with the Riemann ζ function. By carrying out an exact analytic continuation of the semiclassical functional determinant in the complex variable $\hbar^{-1}$, they have derived a new formula for the semiclassical energy eigenvalues similar in form to Eq. (43) but with each term multiplied by a factor involving the complementary error function $\mathrm{erfc}(z_n)$. The quantity z_n corresponding to the nth pseudo-orbit depends on the action $S_n(E)$ and derivatives of $N_{\rm TF}(E)$ with respect to $\hbar^{-1}$. It also depends on a parameter K, the value of which determines how rapidly the pseudo-orbits enter the sum as a function of the energy E. The net effect of this new formulation is to bring about a smoothing of the Riemann-Siegel cutoff defined in Eq. (44). For given E, the center of the smoothing occurs at the pseudo-orbits whose periods are $T_n(E) \approx \pi\hbar d_{\rm TF}(E)$. Further details of this approach are given in Eqs. (70)–(73) of Berry and Keating's paper [22].

The results of calculations for the 49° wedge are shown in Fig. 13. The dotted curve shows the left-hand side of the Riemann-Siegel equation plotted against $Ed_{\rm TF}(E)/3$ over the range of the first 46 energy eigenvalues. The solid dots in the figure are the positions of the exact eigenvalues of the Schrödinger equation. The calculation included 26706 pseudo-orbits having word length ≤ 19. In the same figure the solid curve is the result of the Berry-Keating smoothed version with $K = 50$, employing the same pseudo-orbits. [This calculation was restricted to $\Delta_0(E,\hbar,K)$ given in Berry and Keating's Eq. (72).] The two curves are close to each other, but a careful examination shows that the solid curve has smoothed away the small discontinuities of the dotted curve associated with the abrupt entrance of new orbits satisfying Eq. (44)

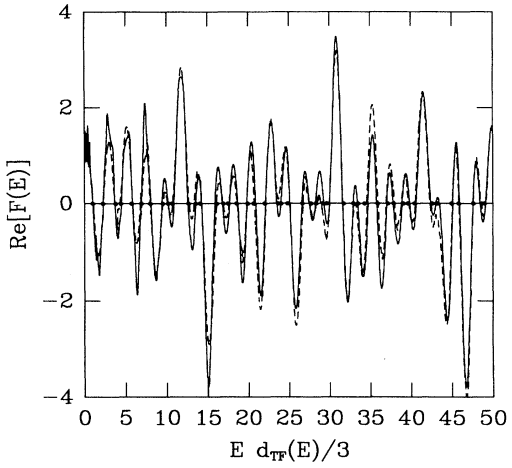

FIG. 13. Calculations for the 49° wedge of the left-hand side of the Riemann-Siegel look-alike equation, Eq. (43), as a function of $Ed_{\rm TF}(E)/3$, with and without smoothing. Both curves contained 26706 pseudo-orbits having word length ≤ 19. The solid curve is the result for the Berry-Keating formulation employing $\mathrm{erfc}(z_n)$ with $K = 50$. The dashed curve is the result for the unsmoothed Riemann-Siegel look-alike equation. The solid circles indicate the positions of the exact energy eigenvalues.

as the energy is increased. However, the Berry-Keating smoothed curve does not miss any eigenvalues or introduce any spurious ones over the range of the first hundred eigenvalues, unlike the dotted curve in the figure, which misses the 21st and 22nd eigenvalues and many pairs of eigenvalues thereafter. We conclude that the Berry-Keating smoothed version of the Riemann-Siegal look-alike equation is successful in determining the first hundred semiclassical energy eigenvalues of the 49° wedge.

E. Cycle expansions

Cycle expansions have been proposed by Cvitanović and co-workers [36–39, 7] as a way of expressing the dynamical ζ function in a properly convergent form. The key idea is to expand the ζ product of Eq. (32) into contributions from a relatively small number of *fundamental cycles*, which are expected to give the dominant contributions, plus *curvature corrections* which are expected to become exponentially small with increasing word length n. In order that a cycle expansion be effective for a particular system, the symbolic dynamics must be *complete* (i.e., there is a 1-1 correspondence between the primitive periodic orbits of the classical system and every unique sequence of symbols, excluding repetitions, cyclic permutations, and time-reversed sequences), or, alternatively, the pruning rules must be known. If the symbolic dynamics is not complete and the pruning rules are not known, then it may not be possible to recast the cycle expansion in a form that converges any better than the Gutzwiller trace formula or the unexpanded ζ product.

In the case of the 49° and 60° wedges, the pruning rules are not completely known at the present time, al-

though some elements of the pruning grammar have been discovered [40]. Nevertheless, it is of interest to show the outcome of a calculation for the 49° wedge which included 162 fundamental cycles and 886 curvature corrections of the form $t_c = t_i - t_j t_k$. The modulus of the resulting ζ function, $|Z(E)|$, calculated as a function of the energy, is shown as the dotted curve in Fig. 14. The solid curve in the figure is $|Z(E)|$ calculated from the product form, Eq. (32), with 1048 primitive periodic orbits having word length ≤ 19. (This is the same curve as in Fig. 10.) As usual, the abscissa in the figure is taken to be $Ed_{\rm TF}(E)/3$, and the triangles indicate the positions of the exact eigenvalues of the Schrödinger equation. Comparing the two curves we see that the cycle expansion does not give as good results as the simple product form. (See, for example, the region of the eighth, ninth, and tenth eigenvalues.)

One can also ask whether better results will be obtained by making use of the functional equation. To study this we have calculated the left-hand side of Eq. (35) as a function of energy for the 49° wedge, with $Z(E)$ calculated as described in the preceding paragraph. The results were found to be considerably improved, but are less satisfactory than the solid curve in Fig. 11 [in which $Z(E)$ is the simple product over 1048 primitive periodic orbits]. For example, we found that the cycle expansion calculation completely misses the 21st and 22nd energy eigenvalues. The anisotropic Kepler problem provides an interesting contrast to this situation since its symbolic dynamics are good, being characterized by a single pruning rule. When its cycle expansion is combined with the functional equation, Tanner and Wintgen and co-workers [5,6] showed that Eq. (35) gives excellent values for the lowest 30 energy eigenvalues. The poor results we have obtained for the 49° wedge, together with the excellent results for the anisotropic Kepler problem, show the importance of knowing the pruning rules and formulating an appropriate cycle expansion along with the functional equation. This is currently being investigated [40].

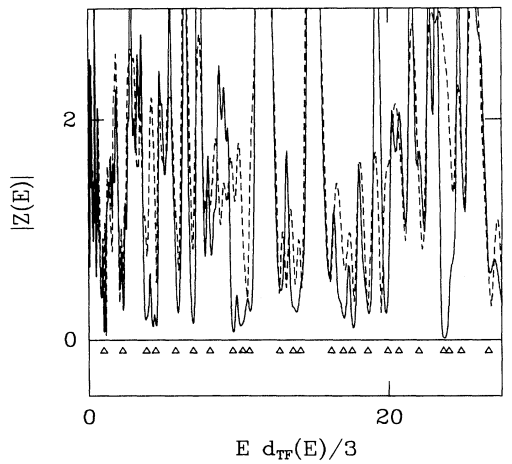

FIG. 14. Comparison of the product form of $|Z(E)|$ with the results of a cycle expansion for $|Z(E)|$ for the 49° wedge. Solid curve: the product form, Eq. (32), calculated with 1048 primitive periodic orbits with word length ≤ 19. Dotted curve: a cycle expansion consisting of 162 fundamental cycles and 886 curvature corrections of the form $t_c = t_i - t_j t_k$. The triangles show the positions of the exact energy eigenvalues of the Schrödinger equation.

F. Expansion in irreducible orbits

There is a puzzling feature of the Gutzwiller trace formula and its reformulation as a ζ product which has not so far been mentioned. The uncertainty principle tells us that it is impossible to resolve the details of the motion of a quantum system on a scale less than that of a Planck cell—a phase space volume of $(2\pi\hbar)^f$, where f is the number of degrees of freedom of the system. The trace formula evidently ignores this fact since it consists of a sum over *all* the periodic orbits of the classical system, and while the primitive periodic orbits with short periods or actions yield the "coarse" features of the classical motion, the orbits having longer periods are expected to describe refinements of that motion on smaller and smaller scales. One wonders, therefore, why there is not a natural cutoff to the periodic orbit sum or the ζ product, which would, of course, depend on the energy of the system.

Recent work by Bogomolny [41, 23, 24], based on a quantum Poincaré surface of section, leads in a natural way to a truncation of the ζ product at precisely the point at which the details of the classical periodic orbits become comparable with the size of a Planck cell. Fundamental to this approach is the concept of an *irreducible orbit*, defined as one in which the classical trajectory does not pass more than once through any Planck cell in the accessible part of the chosen Poincaré surface of section. The net result of this theory is an expansion of the dynamical ζ function in the form of a Dirichlet series consisting of products of the irreducible orbits, the number depending on the number of Planck cells on the Poincaré surface of section. Very nearly the same result will be given by taking $Z(E)$ to be the naive product [6] over the irreducible orbits up to the word length corresponding to the number of Planck cells.

Without going into greater detail, we present here, for the sake of comparison with the approaches described above, the results of a calculation with $Z(E)$ taken to be the naive product over the irreducible orbits up to word length $n \leq 16$. The Poincaré surface of section is taken to be the straight line along the tilted wall of the wedge. A primitive periodic orbit of word length n crosses this line (in a given direction) exactly n times in one period. A description using four-symbol cells [23] corresponds to $2^4 = 16$ Planck cells on the Poincaré surface of section and contains 179 irreducible orbits if none of them are pruned. However, in the case of the 49° wedge, only 16 of these irreducible orbits exist. It is interesting to calculate $Z(E)$ as the hopelessly naive product over these 16 irreducible orbits and find the zeros of the function $\mathrm{Re}[Z(E)\exp(-i\pi N_{\rm TF}(E))]$ plotted against $Ed_{\rm TF}(E)/3$. The result of doing this for the 49° wedge is shown as the dashed curve in Fig. 15. For the sake of comparison, the solid curve corresponds to $Z(E)$ consisting of a product

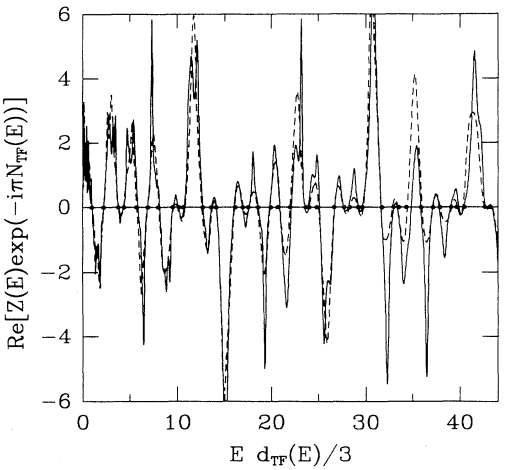

FIG. 15. Comparison between the approach of Bogomolny and calculations employing the functional equation for the 49° wedge. Dashed curve: $Z(E)$ calculated as the simple product containing only the 16 irreducible orbits that exist for word length $n \leq 16$. Solid curve: $Z(E)$ calculated as the product of the 363 primitive periodic orbits that exist for word length $n \leq 16$. In both cases what is plotted is $\mathrm{Re}\{Z(E)\exp[-i\pi N_{\mathrm{TF}}(E)]\}$ against $Ed_{\mathrm{TF}}(E)/3$. The positions of the exact eigenvalues of the Schrödinger equation are indicated by the solid circles.

over the 363 primitive periodic-orbits that exist up to code length 16. It may be seen that for both curves the zeros are very close to the positions of the exact energy eigenvalues.

VIII. SUMMARY AND DISCUSSION

The main objective of the present investigation was to study a number of different ways of calculating approximate energy eigenvalues for the wedge billiard using periodic-orbit theory. The results, taken in conjunction with the results of similar calculations for the anisotropic Kepler problem, the model of a particle moving on a surface of constant negative curvature, and the hyperbola billiard, may help to establish which quantization rule gives the best predictions.

The various methods may be compared by calculating the deviations of the lowest 30 semiclassical energies from the exact eigenvalues of the Schrödinger equation. The results for the 60° wedge are shown in Table I. With $\tilde{E} = Ed_{\mathrm{TF}}(E)/3$, the first column of numbers in the table gives the mean deviation $\langle \tilde{E}_i - \tilde{E}_i^{\mathrm{exact}} \rangle$, while the second column gives the root-mean-square deviation $\langle (\tilde{E}_i - \tilde{E}_i^{\mathrm{exact}})^2 \rangle^{1/2}$. The final column states the number of energy eigenvalues among the lowest 30 that were used in these calculations, since two quantization schemes did not locate all the eigenvalues unambiguously. The straight Thomas-Fermi predictions (without the oscillatory corrections) provide a "worst case" value for the rms deviation against which the other calculations may be compared. A clear winner for the 60° wedge is the calculation of the zeros of $\mathrm{Re}\{\exp[-i\pi N_{\mathrm{TF}}(E)Z(E)\}$ where $Z(E)$ is the simple ζ product with 1621 primitive periodic orbits. Not far behind is the staircase quantization scheme which also gives very good results for the lowest 30 energy eigenvalues.

Similar results for the 49° wedge are shown in Table II. Because the special "vertex orbits" of the 60° wedge do not exist in this case, there is no difficulty in carrying out the various expansions of the dynamical ζ function in the form of a Dirichlet series. Here too the straight Thomas-Fermi quantization $N_{\mathrm{TF}}(E_j) = j - 1/2$ provides a "worst case" value with which to compare the rms deviation. Among the quantization schemes that predict *all* of the lowest 30 energy eigenvalues, without introducing any spurious ones, the best results are given by Bogomolny's approach—the hopelessly naive product over the 16 irreducible orbits corresponding to 4-symbol cells, together with the functional equation. Almost as good, however, are the results obtained using the merely naive product over 363 or 1048 primitive periodic orbits together with the functional equation.

Our study of various quantization schemes for the wedge billiard supports the conclusion reached by Tanner and Wintgen [6] on the basis of their recent investigation of the anisotropic Kepler problem. They found that the best results were obtained by the Bogomolny approach employing 3-symbol cells, with the straight ζ product plus the functional equation being nearly as good. In the anisotropic Kepler problem only one orbit is pruned, in contrast to the extensive pruning that occurs for the wedge billiard. It appears from our results that even when the pruning is severe, the Bogomolny approach with a small number of irreducible periodic orbits still gives very good results for the approximate energy eigenvalues. Thus, our results in conjunction with those of

TABLE I. Comparison of the mean deviation and the root-mean-square deviation of the calculated energy eigenvalues from the exact eigenvalues of the Schrödinger equation for the 60° wedge. Fewer than 30 eigenvalues were used in two cases because the quantization schemes did not unambiguously locate all the eigenvalues. Except for the Thomas-Fermi energy levels (which require no periodic orbits for their calculation), each quantization scheme employed 1621 primitive periodic orbits. Note that $\tilde{E} = Ed_{\mathrm{TF}}(E)/3$.

Quantization scheme	Figure	$\langle \tilde{E}_i - \tilde{E}_i^{\mathrm{exact}} \rangle$	$\langle (\tilde{E}_i - \tilde{E}_i^{\mathrm{exact}})^2 \rangle^{1/2}$	Number of eigenvalues
Gutzwiller sum	5	-0.019	0.107	27
Thomas-Fermi	8	0.085	0.224	30
Staircase quantization	8	-0.108	0.058	30
$Z(E)$ product form	9	-0.004	0.121	25
$Z(E)$ product & func. rel.		-0.031	0.040	30

TABLE II. Comparison of the mean deviation and the root-mean-square deviation of the calculated energy eigenvalues from the exact eigenvalues of the Schrödinger equation for the 49° wedge. For certain calculations, fewer than 30 eigenvalues were used because the quantization scheme did not unambiguously locate all the eigenvalues. The values in parentheses give the number of primitive periodic orbits or pseudo-orbits used in the calculations. Note that $\tilde{E} = Ed_{\rm TF}(E)/3$.

Quantization scheme	Figure	$\langle \tilde{E}_i - \tilde{E}_i^{\rm exact} \rangle$	$\langle (\tilde{E}_i - \tilde{E}_i^{\rm exact})^2 \rangle^{1/2}$	Number of eigenvalues
Gutzwiller sum (1048)	4	0.077	0.152	29
Thomas-Fermi (0)		0.014	0.333	30
Staircase quantization (1048)		-0.284	0.215	30
$Z(E)$ product form (1048)	10	0.072	0.118	24
$Z(E)$ product & func. rel. (1048)	11	0.029	0.113	30
$Z(E)$ pseudo orbits & func. rel. (26706[a])	11	0.046	0.126	30
Riemann-Siegel look-alike (26706[a])	13	0.014	0.104	20
Berry-Keating erfc, K=50 (26706[a])	13	0.028	0.142	30
Quantum PSOS (16 irreducible)[b]	15	0.017	0.100	30
$Z(E)$ product & func. rel. (363)[c]	15	0.028	0.109	30

[a]All pseudo-orbits with word length ≤ 19.

[b]There are 16 irreducible orbits with word length ≤ 16.

[c]There are 363 primitive periodic orbits with word length ≤ 16.

Tanner and Wintgen indicate that the product form of $Z(E)$ plus the functional equation performs better than any of the approaches which express $Z(E)$ as a Dirichlet series. It is not at all clear why this should be so.

ACKNOWLEDGMENTS

This research was supported by the Natural Sciences and Engineering Research Council of Canada. Calculation of the energy eigenvalues was made possible by a generous provision of time on the Cray X-MP at the Ontario Centre for Large Scale Computation. We would like to thank J. Keating for correspondence concerning the key equations in Ref. [22]. We would also like to thank M. Berry, E. Bogomolny, J. Lefebvre, V. Snaith, F. Steiner, and M. Wang for helpful discussions on various aspects of this work.

[1] M.C. Gutzwiller, J. Math. Phys. **12**, 343 (1971).
[2] M.C. Gutzwiller, *Chaos in Classical and Quantum Mechanics* (Springer-Verlag, New York, 1990).
[3] T. Szeredi and D.A. Goodings, Phys. Rev. Lett. **69**, 1640 (1992).
[4] M.C. Gutzwiller, Physica D **5**, 183 (1982).
[5] G. Tanner, P. Scherer, E.B. Bogomolny, B. Eckhardt, and D. Wintgen, Phys. Rev. Lett. **67**, 2410 (1991).
[6] G. Tanner and D. Wintgen, CHAOS **2**, 53 (1992).
[7] F. Christiansen and P. Cvitanović, CHAOS **2**, 61 (1992).
[8] R. Aurich, M. Sieber, and F. Steiner, Phys. Rev. Lett. **61**, 483 (1988).
[9] R. Aurich and F. Steiner, Physica D **39**, 169 (1989).
[10] R. Aurich and F. Steiner, Physica D **43**, 155 (1990).
[11] M. Sieber and F. Steiner, Physica D **44**, 248 (1990).
[12] M. Sieber and F. Steiner, Phys. Rev. Lett. **67**, 1941 (1991).
[13] M. Sieber, DESY Report No. 91-030 (1991) (unpublished).
[14] M. Sieber, CHAOS **2**, 35 (1992).
[15] R. Aurich and F. Steiner, Phys. Rev. A **45**, 583 (1992).
[16] M.C. Gutzwiller, in *Stochastic Behavior in Classical and Quantum Hamiltonian Systems*, edited by G. Casati and J. Ford (Springer, Berlin, 1979), p. 316.
[17] M.V. Berry, in *Quantum Chaos and Statistical Nuclear Physics*, edited by T.H. Seligman and H. Nishioka, Lecture Notes in Physics Vol. 263 (Springer, Berlin, 1986), p. 1.
[18] M.C. Gutzwiller, J. Phys. Chem. **92**, 3154 (1988).
[19] A. Voros, J. Phys. A **21**, 685 (1988).
[20] M.V. Berry and J.P. Keating, J. Phys. A **23**, 4839 (1990).
[21] J.P. Keating, Proc. R. Soc. London Ser. A **436**, 99 (1992).
[22] M.V. Berry and J.P. Keating, Proc. R. Soc. London Ser. A **437**, 151 (1992).
[23] E. Bogomolny, CHAOS **2**, 5 (1992).
[24] E. Bogomolny, Nonlinearity **5**, 805 (1992).
[25] A. Wittek, doctoral dissertation, University of Bremen (1991) (unpublished).
[26] T. Szeredi, Ph.D. thesis, McMaster University (1992) (unpublished).
[27] D.A. Goodings and T. Szeredi, Am. J. Phys. **59**, 924 (1991).
[28] M.V. Berry and M. Tabor, Proc. R. Soc. London Ser. A **356**, 375 (1977).
[29] O. Bohigas, M.J. Giannoni, and C. Schmit, Phys. Rev. Lett. **52**, 1 (1984).
[30] O. Bohigas, M.J. Giannoni, and C. Schmit, J. Phys. Lett. **45**, L1015 (1984).
[31] B. Eckhardt and E. Aurell, Europhys. Lett. **9**, 509 (1989).
[32] M. Sieber and F. Steiner, Phys. Lett. A **144**, 159 (1990).
[33] M. Kac, Am. Math. Mon. **73**, 1 (1966).
[34] F. Steiner and P. Trillenberg, J. Math. Phys. **31**, 1670

(1990).
[35] C. Matthies and F. Steiner, Phys. Rev. A **44**, R7877 (1991).
[36] P. Cvitanović, Phys. Rev. Lett. **61**, 2729 (1988).
[37] P. Cvitanović and B. Eckhardt, Phys. Rev. Lett. **63**, 823 (1989).
[38] R. Artuso, E. Aurell, and P. Cvitanović, Nonlinearity **3**, 325 (1990); **3**, 361, (1990).
[39] P. Cvitanović, Physica D **51**, 138 (1991).
[40] P. Cvitanović and K. Hansen (unpublished).
[41] E. Bogomolny, Comm. At. Mol. Phys. **25**, 67 (1990).